# Off-Line Signature Verification by Local Granulometric Size Distributions

Robert Sabourin, *Member, IEEE*, Ginette Genest, and Françoise J. Prêteux

**Abstract**—A fundamental problem in the field of off-line signature verification is the lack of a signature representation based on shape descriptors and pertinent features. The main difficulty lies in the local variability of the writing trace of the signature which is closely related to the identity of human beings. In this paper, we propose a new formalism for signature representation based on visual perception. A signature image consists of $512 \times 128$ pixels and is centered on a grid of rectangular retinas which are excited by local portions of the signature. Granulometric size distributions are used for the definition of local shape descriptors in an attempt to characterize the amount of signal activity exciting each retina on the focus of the attention grid. Experimental evaluation of this scheme is made using a signature database of 800 genuine signatures from 20 individuals. Two types of classifiers, a Nearest Neighbor and a threshold classifier, show a total error rate below 0.02 percent and 1.0 percent, respectively, in the context of random forgeries.

**Index Terms**—Off-line signature verification, feature extraction, shape analysis, mathematical morphology.

## 1 Introduction

In the field of pattern recognition, off-line signature verification is still an open problem [15], [24], [28]. Moreover, the complete elimination of random forgeries, defined as genuine signatures of other writers enrolled in the verification system, is a prerequisite for real applications. A brief analysis reveals that this is a very easy task for human beings, especially because no attempt to imitate the target signature is involved for this class of forgeries [25]. We would like to know why this pattern recognition task is so difficult to automate successfully.

During a period of more than 20 years of active research, several approaches have been proposed and evaluated in the context of random forgeries, like 2D transforms [22], histograms of directional data [11], [12], [36] or curvature [5], horizontal and vertical projections of the writing trace of the signature [1], structural approaches [27], [31], local measurements made on the writing trace of the signature [21] and the position of feature points located on the skeleton of the signature [26]. The best experimental results have been reported in [32] where a total error rate of one percent has been obtained with our signature database and experimental protocol. Despite the fact that experimental results from other works are difficult to compare because no international database is available in this field due to the confidentiality problems with this type of data, it should be possible to achieve a perfect recognition rate for real applications considering this class of (random) forgeries.

A survey of the most popular schemes in the literature suggests that a new way of addressing the problem of signature verification be formulated in order to find a satisfactory solution for eliminating random forgeries. One possibility consists of analyzing the intrinsic characteristics of genuine signatures. Following Plamondon [24], a handwritten signature is the result of a rapid movement. Hence, the shape of the signature remains relatively the same over time when the signature is written down on a pre-

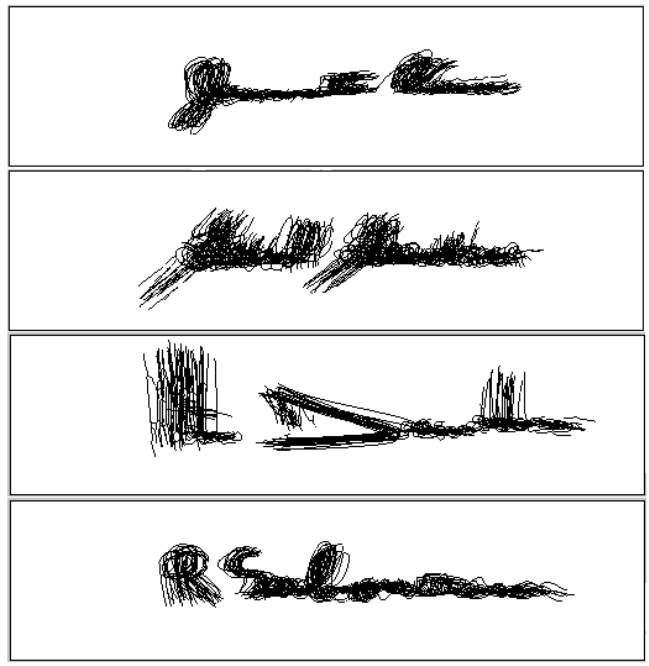

Fig. 1. Twenty skeletons of genuine signatures from four writers centered and superimposed in the image plane.

- *R. Saborin and G. Genest are with the Laboratoire d'Imagerie, de Vision et d'Intelligence Artificielle (LIVIA), École de technologie supérieure, Département de génie de la production automatisée, 1100, rue Notre-Dame Ouest, Montréal, Québec, H3C 1K3, Canada. E-mail: sabourin@gpa.etsmtl.ca.*
- *F. Prêteux is with the Institut National des Télécommunications, Département Signal et Image, 9 rue Charles Fourier, 91011 Évry, France. E-mail: preteux@int-evry.fr.*

*Manuscript received 18 Apr. 1996; revised 7 July 1997. Recommended for acceptance by J.J. Hull.*
*For information on obtaining reprints of this article, please send e-mail to: tpami@computer.org, and reference IEEECS Log Number 105405.*

established frame (context) like a bank check. This physical constraint contributes to the relative time-invariance of the signatures. Despite this temporal and spatial "stability," a fundamental problem in the field of off-line signature verification is the lack of a pertinent shape descriptor. The main difficulty in the definition of pertinent features lies in the local variability of the writing trace of the signature which is closely related to the identity of the writer [13], [17]. As an example, 20 skeletons of genuine signatures from four writers have been centered and superposed in Fig. 1. We can see that the global aspect and the overall orientation of genuine signatures are relatively consistent for all writers, but the local position of strokes varies greatly from one signature to the other. The question is, how can the local variability of the signature be taken into account in the definition of a shape descriptor for verification purposes?

Traditionally, there are two classes of shape descriptors: information-preserving (IP) and information-nonpreserving (INP) [16]. IP shape descriptors have the advantage of keeping all the information from the original signature; consequently, an inverse transformation exists and the original shape can be recovered from the descriptor. As an example, the 2D Hadamard transform, an IP descriptor, has been used for signature verification [22]. By contrast, one cannot recover the original shape from INP descriptors. Some examples of INP shape descriptors include the directional probability density function [12], invariant moments, polar sampling of the silhouette of the signature [27], [29] and the envelope of the signature [23].

Although, if IP is a nice property for any shape descriptor in pattern recognition, IP shape descriptors show the worst performances in the context of signature verification. Experts in the field of forensic science make use of local "peculiarities" of handwriting for the authentication of signatures [13], [17]. Moreover, the choice of features is made dynamically according to the type of handwriting to be analyzed [25]. Also, IP shape descriptors systematically take into account the entire image in the process of feature extraction and this does not coincide with the methodology of the experts. Global and local approaches to the definition of a shape descriptor tailored for the signature verification problem can be related to IP and INP properties; global shape descriptors are either IP or INP, while local shape descriptors are normally classified as INP. The main difficulty related to the local analysis of the signature is the need to segment pertinent parts of the signature in an attempt to make some local measurements of the shape. This is a very difficult task [27], [31] and is the motivation for the new approach presented here.

## 2 Formal Model for the Definition of Signature Representation

We propose in this paper, a new formalism for the definition of a signature representation based on visual perception. As mentioned above, local approaches are better suited for defining signature representations than global ones. Based on the observations made earlier on the superposition of genuine signatures (Fig. 1), the following assumptions can be made with respect to defining a shape descriptor tailored for the signature verification problem:

1) *The overall orientation and the overall proportions of genuine signatures written in a constrained 2D area are relatively stable for each writer, and*
2) *The local variability of the writing trace of the signature is an intrinsic characteristic of the identity of the writer and should be taken into account as well. This phenomenon is characterized by local displacements of strokes following the principal axis of the signature.*

From these assumptions, a certain invariance in rotation and in scale results; hence, their explicit requirement is not needed in the definition of a shape descriptor. Only a correction in translation remains necessary. Despite the fact that only four writers have contributed to the examples depicted in Fig. 1, Assumption 1 is in accordance with the opinion of expert examiners in the field of forensic science [13], [17], [25]. Finally, North American signatures are "cursive" in nature; this could partially explain the fact that their overall proportions are relatively stable over time.

The originality of the proposed approach is that local measurements $m(\cdot)$ are not made on specific parts (primitives) of the signature, but on specific areas around foci of attention in the image plane. The identification and segmentation of feature points or primitives on the writing trace of the signature are performed by just assuming that the foci of attention are specified arbitrarily in the image space. This leads to a simplification of the training phase of the verification system. The method proposed here for feature extraction is simple. A signature image of $512 \times 128$ pixels is centered on a grid of rectangular retinas which are excited by local portions of the image (Fig. 2); each retina has only a local perception of the entire scene (Fig. 3), and the measurement $m(\cdot)$ made on the subset $X$ of pixels related to a specific retina will reflect the local activity of the signal.

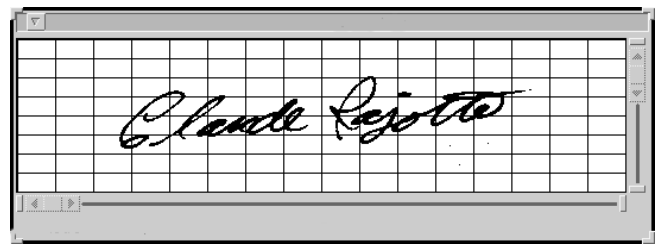

Fig. 2. A signature image centered on a grid of rectangular retinas $W$ of $32 \times 16$ pixels (without overlap).

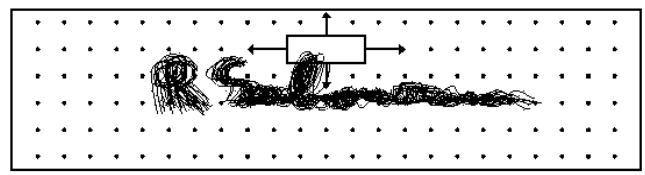

Fig. 3. A rectangular retina $W$ is shown with the field of points of attention uniformly distributed in the image space.

The definition grid (i.e., the position and the number of foci) together with the size of retinas have a great impact on the performance of this approach and a prototyping phase is necessary [see Section 5.1]. An important aspect for signature representation is that the consistent absence of signal activity in specific areas of the image will be taken into account in an attempt to characterize the shape of the signature. This is achieved by Assumption 1 which stated that the overall proportions of genuine signatures are relatively stable. In other words, not only the signature itself but the background also are considered in the definition of the shape descriptor.

From Assumption 2, the local variability of the writing trace of the signature could be taken into account easily by adding a certain percentage of horizontal and/or vertical overlap between neighboring retinas. As the visual observations made on examples depicted in Fig. 1 showed that in general the displacement of strokes follows the principal axis of the signature, this fact suggests that horizontal overlap alone is enough.

The measurement $m(\cdot)$ applied to the set $X$ of pixels related to a retina should be capable of detecting the presence, or absence, of any signal activity, and it should be capable in some way of quantifying it. We now address the specification of $m(\cdot)$. We think that $m(\cdot)$ should be capable of describing the information contained in a binary image and the manner in which it is distributed between the "fine" and "coarse" details. The morphological operations of opening and closing are useful for this task. The *pattern spectrum* is an internal INP morphological shape descriptor called the *pecstrum* [18]. The pecstrum is computed by measuring the result of successive morphological openings of the image, as the size of the structuring element increases. The sequences of openings so obtained are called granulometries [19], [35]. Serra has introduced the complete pattern spectrum, including the negative part of the pecstrum resulting from the sequence of closings of the object under study and using the same family of increasing by large structuring elements. Maragos has extended the pecstrum to gray-level images [18]. A great deal of work related to the use of the pecstrum as a global shape descriptor has been done; see for example [2], [3], [6], [34]. Dougherty used the positive pattern spectrum evaluated in a square area centered around each gray-level pixel to characterize the image pixels for implementing some local segmentation schemes [8], [9], [10]. The technique, which is related to the evaluation of a pattern spectrum for each image pixel, was called "local granulometric size distribution" in [9]. Our objective is to extend this approach of local granulometric size distributions to the definition of local shape descriptors in an attempt to characterize the amount of signal activity exciting each retina on the focus of the attention grid (Figs. 2-3).

## 3 Local Granulometric Size Distributions as a Local Shape Descriptor

### 3.1 Basic Definitions of Morphological Operators

Mathematical morphology is a set theoretical approach for the analysis of geometric structures. Erosion and dilation are the basic morphological operators [35]. The *eroded* set of $X$ with respect to the structuring element $B$, denoted by $X \ominus B^{v}$, is defined as all points $z \in E$ for which the translates $B_z$ are included in $X$:

$$X \ominus B^{v} = \{z \in E : B_Z \subset X\} \tag{1}$$

where $B^{v}$ denotes the symmetrical set of $B$ with respect to the origin of the plane $E$, and $\ominus$ denotes the Minkowski subtraction. The *dilation* of $X$ with respect to $B$ consists of all points $z \in E$ for which the translates $B_z$ hit $X$:

$$X \oplus B^{v} = \{z \in E : B_Z \cap X \neq \varnothing\} \tag{2}$$

where $\oplus$ denotes the Minkowski addition. An erosion followed by a dilation using the same *structuring element* (SE) gives a new morphological operator called an *opening* of $X$ with respect to $B$, denoted by $X_B$, and corresponds to the union of all the translates $B_Z$ of $B$ that lie inside $X$ :

$$\left(X \ominus B^{v}\right) \oplus B = X_B = \bigcup \{B_z : B_z \subset X\} \tag{3}$$

The *closing* of $X$ with respect to the SE $B$, denoted by $X^B$, is the composition of a dilation followed by an erosion using the same SE. Notice that opening and closing are dual operators with respect to the complement operator:

$$\left(X \oplus B^{v}\right) \ominus B = X^B = \left[\left(X^c\right)_B\right]^c \tag{4}$$

where $X^c$ denotes the complement set of $X$. A sequence of increasing by large openings of a set $X$ with respect to the family of SE $rB$ defines a *granulometry*. For a formal definition of a granulometry see [19] and [35].

The *pecstrum* is the result of successive applications of morphological operators on a set using an increasing by large structuring element $rB$. Opening a signal with a structuring element of size $r$ can be viewed as removing details smaller than $rB$ from the signal. The digital version of the pecstrum is defined as [2]:

$$p(n) = \frac{m\left(X_{nB}\right) - m\left(X_{(n+1)B}\right)}{m(X)},\ n = 0, 1, \ldots, k-1 \tag{5}$$

with

$$\sum_{n=0}^{k} p(n) = 1 \tag{6}$$

Each $p(n)$ represents the fraction of the total area of $X$ that is rejected by the opening with the SE $(n+1)B$ provided that the opening with $nB$ has already been performed. The SE used is the integer multiple $(nB)$ of a basic prototype $B$. The value $n = k - 1$ is the one for which a binary object disappears after it has been opened with $kB$. In other words, a single impulse at $p(n) = 1$ means that the binary object totally disappears because of the SE $(n+1)B$. The pecstrum is translation and rotation invariant (considering the limit of a square lattice), but it is not scale invariant. The latter property

is not critical in our methodology because the granulometries were evaluated on retinas in the image that were of the same size, that is to say, the dimensions of the retinas are all the same (Fig. 2) leading to a local normalization of the image and the measurement.

The negative part of the pecstrum is obtained by measuring the change in the area of the object when successive closings are performed on it [2]:

$$p(-n) = \frac{m\left(X^{nB}\right) - m\left(X^{(n-1)B}\right)}{m(X)},\ n = 1, \ldots, k \qquad (7)$$

Following Serra [35], successive closings of an object approximate its convex hull and the final result varies depending on the shape of the SE used. The negative part of the pattern spectrum relates to some normalized measure of the size of the holes and cavities in the object. The first components of both the positive and the negative pecstrum contain information about the boundary roughness of the object. The major drawback of the negative spectrum, from a computational point of view, lies in the difficulty of properly determining the maximum value of $n$, e.g., the value $k$ [2], [6].

The *pseudopecstrum* $p_s$ was introduced by Anastassopoulos in [2] as a solution to the computational problems of the negative part of the pecstrum. The pseudopecstrum $p_s$ of a binary object $X$ is the ordinary positive pecstrum of the complement $X^c$, relative to the minimum circle which has its center in the center of gravity of $X$ and contains $X$. The values $p_s(n)$ are normalized using the original area of the object $X$, and the shape of the SE is assumed to be circular. The process of evaluating $p_s$ terminates when the area of $X^c$ becomes zero. The information content of the pseudopecstrum is not the same as that contained in the negative pecstrum. The pseudopecstrum contains information about the cavities and holes in the object $X$, but also measures whether or not the object is similar to a circle. The pseudopecstrum contains some misleading shape information, especially in its first components which come from the regions where the circumscribed circle touches the object $X$. In summary, the pseudopecstrum yields the distribution of the analyzed scene in shape and size; the corresponding measurements depend on the SE.

### 3.2 Definition of a Local Signature Representation

Using the concept of shape descriptors tailored for the signature-verification problem based on visual perception [Section 2], the amount of signal activity from a retina can be characterized in different ways using morphological operators. We formally define each retina as the set $W$ of pixels in the area covered by the retina located at a specific point of attention in the image (Fig. 4). Let $X$ be the set of pixels belonging to the signal exciting the retina. As an example, the set $X$ shown in Fig. 4 is defined as the four pieces of the signature in the field of view of a rectangular retina $W$, with $X = \bigcup_{i=1}^{4} \{X_i\} \subseteq W$. It is clear that $X = \varnothing$ when no signal activates the retina. Finally, the set $E$ represents the *augmented set* $W$ used in some experiments with the purpose of eliminating some noise characterized by pixels belonging to $X$ and located in the neighborhood of the external border of set $W$. Here, no signal activity is present in the surroundings of $W$, that is, in the area $(E \cap W)^c$.

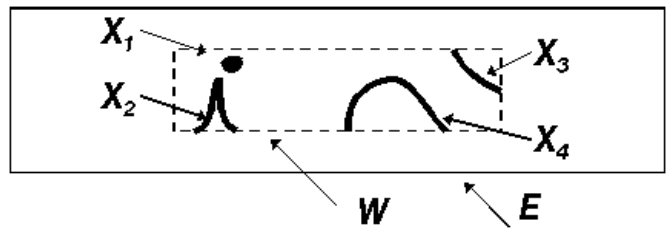


Fig. 4. Definition of $W$ the set of pixels related to the local field of view of a rectangular retina.

Many alternatives were tried in this work in an attempt to define a measurement $m(\cdot)$ of the local activity of signal $X$ which activates a retina $W$. First, the *positive pecstrum* was used as a transform $\Psi p(X)$ applied to the set $X$ of signal pixels included in $W$, with $W = E$ and $(W \cap E)^c = \varnothing$. No border effects are anticipated in this case, so it is not necessary to increase the basic retina area. Second, the *pseudopecstrum* $\Psi p_s(X^c)$ was applied to $X^c$ (the complement of $X$ with respect to the domain defined by set $E$, with $W = E$). When the SE used for the transformation $\Psi p_s(X^c)$ is one of the segments in the set {—, |, /, \}, then set $E$ is a rectangular area as depicted in Fig. 4 with $W = E$. When a circular SE is used for the transformation $\Psi p_s(X^c)$, then $E$ corresponds to the circular area defined by the circumscribing circle to $W$ (Fig. 5b). In both cases, $\Psi p_s(\cdot)$ is applied to $X^c \subseteq E$, whatever the choice of SE.

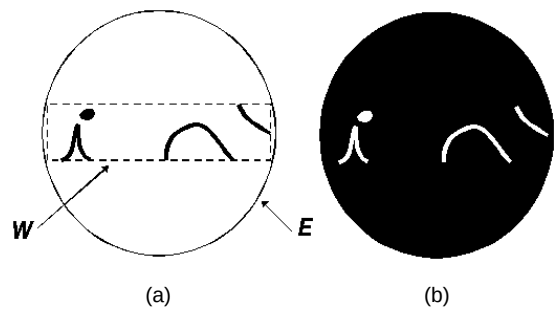


Fig. 5. Example of a set $X^c$. (b) The complement of $X$ in the circular domain defined by set $E$ (a).

Finally, the *augmented pseudopecstrum* $\Psi ap_s(X^c)$ is simply the pseudopecstrum based on an SE in {—, |, /, \} and applied to $X^c$, the domain defined by $E$, with $X \subseteq W \subset E$, $(W \cap E)^c \neq \varnothing$ and $X^c \subseteq E$. In this case, a scale factor of 50 percent in the horizontal and vertical directions is used in the definition of $E$ when the augmented pseudopecstrum is considered (Fig. 4). As an example, a set W related to a rectangular area of $32 \times 16$ pixels gives the augmented set $E$ with a cardinality $|E| = 64 \times 32$ pixels. In the case of a

circular $E$, the increase in area is not necessary because the shape of the SE and that of $E$ are the same; no border effects can occur in this case. The field of view of a retina is directly proportional to its size; this factor has a great impact on the performance of the verification system. In Table 1, the horizontal ($h$) and the vertical ($v$) length, in pixels, of a retina permit the direct evaluation of $|W|$. The horizontal and vertical dimensions of the signature images are 512 and 128 pixels, respectively; the number of retinas $n_r$ can be evaluated from the product $n_h * n_v$, where $n_h$ and $n_v$ correspond to the number of retinas in the horizontal and vertical directions respectively. In Table 1, $n_h = 512 / h$, $n_v = 128 / v$, and $|W| = h \times v$.

TABLE 1
BASIC DEFINITION OF RETINA W (IN PIXELS)

| $h \times v$ | $n_h$ | $n_v$ | $n_r$ | $n$ |
|---|---|---|---|---|
| $16 \times 16$ | 32 | 8 | 256 | 768 |
| $16 \times 32$ | 32 | 4 | 128 | 384 |
| $32 \times 16$ | 16 | 8 | 128 | 384 |
| $32 \times 32$ | 16 | 4 | 64 | 192 |
| $64 \times 32$ | 8 | 4 | 32 | 96 |

The resulting signature representation $\mathcal{X}_i$ is a feature vector of dimension $n$ equal to the product $n_r$ * LD, where LD is the number of local shape descriptors evaluated from a retina and $n_r$ the number of retinas applied to the entire image. Here, the granulometric moments have been used as local shape descriptors resulting from the evaluation of measurements m(·) of a specific transformation $\Psi(\cdot)$ applied to set $E$, where $E \rightarrow \Psi(E) \rightarrow m(\Psi(E))$. For each retina, the granulometric moments (LD = 3 in this case) are evaluated for the positive pattern spectrum as:

$$\text{the mean} \quad \mu = \frac{\left(\sum_{n=0}^{k-1} n \cdot p(n)\right)}{area(X)} \tag{8}$$

$$\text{the variance} \quad \sigma^2 = \frac{\left(\sum_{n=0}^{k-1} (n-\mu)^2 \cdot p(n)\right)}{\left(area(X)-1\right)} \tag{9}$$

$$\text{the skewness} \quad \alpha = \frac{\left(\sum_{n=0}^{k-1} (n-\mu)^3 \cdot p(n)\right)}{\left(\sigma^3 \cdot area(X)\right)} \tag{10}$$

of the distribution $p(n)$, where $area(X)$ is the area in pixels of set $X$. Consequently, the dimension $n$ of the feature space $\Re^n$ is equal to 3 * $n_r$ as shown in Table 1. A value of $n = 768$ represents a very high feature space, which is normally intractable in the context of a standard pattern recognition problem. The reason why a high dimension like this one has been used for the signature verification problem, given that the number of observations available for training is very low, is that a

(a)

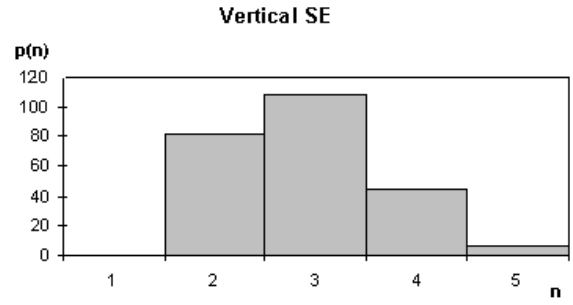


(b)

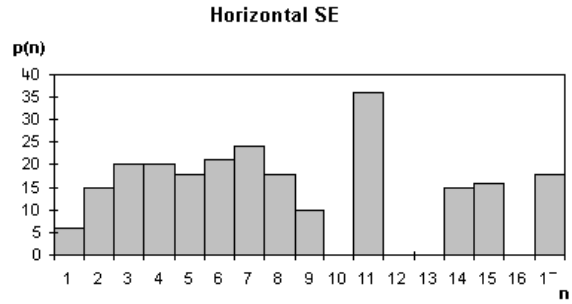


(c)

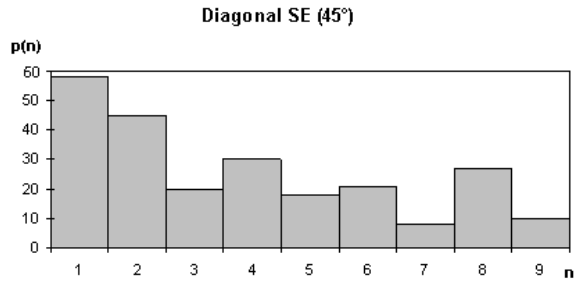


(d)

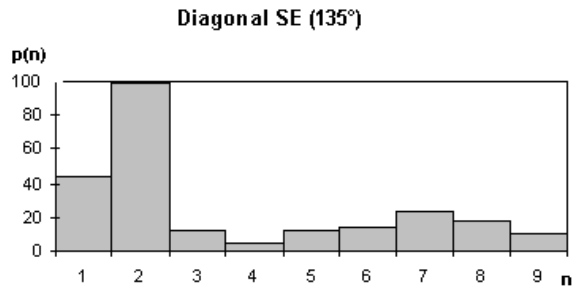


(e)

Fig. 6. A signature image (a) and the pecstrums $\Psi p(X)$ based on SE in {|, —, /, \} with $E = W$ are depicted in (b) to (e).

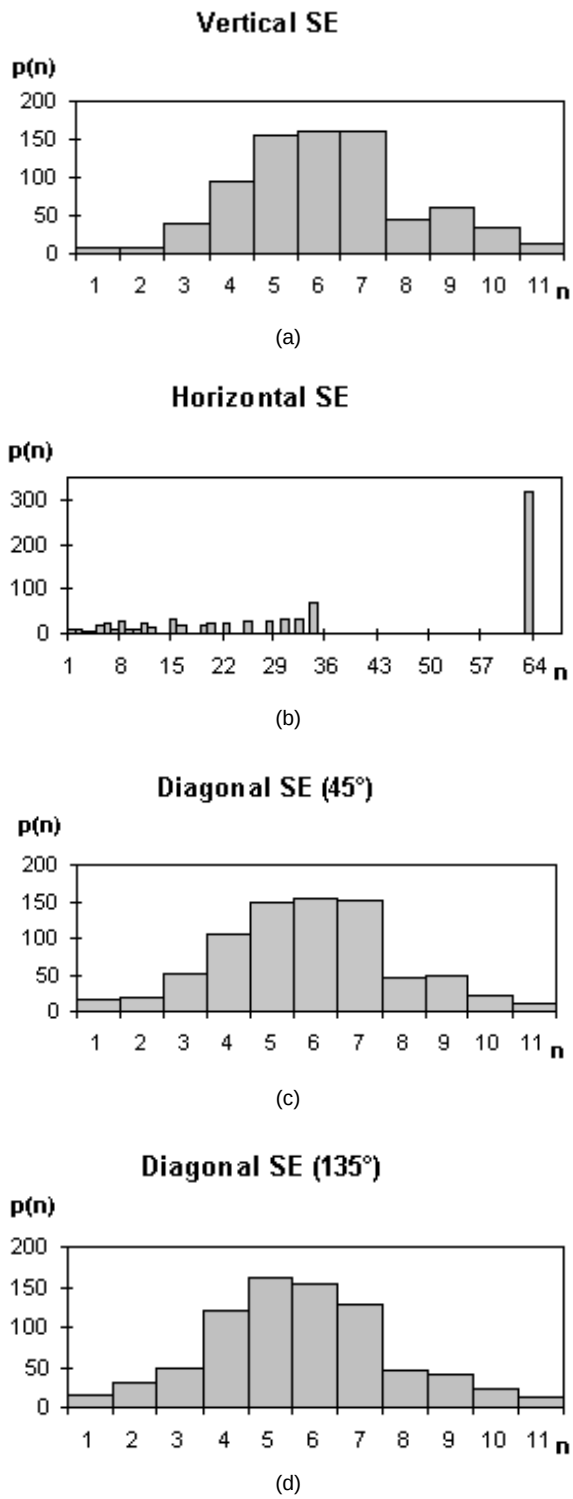


Fig. 7. Pseudopecstrums $\Psi p_S(X^C)$ based on SE in {|, —, /, \} ((a) to (d)) have been evaluated on the same retina $W$ shown in Fig. 6a with $W = E$.

large number of retinas are not excited by the signal. Consequently, a lot of elements in the feature vectors have a fixed value. As an example, only 40 of the 128 retinas shown in Fig. 2 were excited by parts of the signature.

### 3.3 Examples of Transformations Ψ(·) Applied to Handwritten Signatures

Some examples of transformations $\Psi(\cdot)$ applied to a rectangular retina $W$ with $h = 32$ and $v = 16$ pixels and 50 percent of overlap in the horizontal direction ($|W| = 64 \times 16$ pixels [Fig. 6a]) are discussed in this section. No extended area was used in this case; consequently $E = W$. The set $X$ which activates the retina $W$ represents a horizontal covering of the stroke in the entire area of $W$. The pecstrums $\Psi p(X)$, based on SE from the set {|, —, /, \}, (with $E = W$), are shown in Fig. 6b to Fig. 6e. In this case, the pattern spectrum related to the vertical SE characterizes the thickness of the stroke (Fig. 6b). This is because no loops are present in front of the retina area. The horizontal SE reveals the presence of curves in the area, and this is taken into account by the spread of $p(n)$ values over the entire spectrum (Fig. 6c). Here, the strength of impulses p(n) located at the end of the scale relate in a certain way to the horizontal regularity of the stroke. The diagonal SE {/, \}, permits measurement of the slope of short sections of the writing trace of the signature appearing in $W$. The presence of this type of stroke will be represented by $p(n)$ values located at the end of the spectra. By contrast, the presence of a horizontal straight line will result in a distribution like the one obtained with the vertical SE; the impulses p(·) will then be located near the origin of the spectra.

The pseudopecstrums $\Psi p_s(X^c)$ based on SE in {|, —, /, \} were evaluated on the same retina $W$ as shown in Fig. 6a with $W = E$; the results are depicted in Fig. 7. Transformations $\Psi(\cdot)$ are now applied to $X^c$; this permits indirect measurement of the amount of signal activity based on the background analysis. In this example, the stroke $X$ covered the entire horizontal part of the retina. This phenomenon is reflected in spectra based on SE in {|, /, \} by the absence of impulses $p(n)$ located at the end of the scale (Figs. 7a, 7c and 7d). Moreover, the spread of all three spectra is very low; this is a good indication of the continuity of the writing trace of the signature. The shape of the distributions also reveals some stroke irregularities; for example, for the vertical SE, the presence of a long horizontal straight line will give two impulses whose strength and position in the spectrum depend on the vertical position of the line in $W$. Following the study of the pseudopecstrum based on the horizontal SE depicted in Fig. 7b, the presence of a strength impulse $p$(n) at position $n = 64$ gives some information about the partial covering of the signal $X$ in the vertical direction. In this instance, the spread of the spectrum also reflects the irregularities of the writing trace of the signature.

The pseudopecstrum $\Psi p_s(X^c)$ based on a circular SE was applied to the same retina $W$ depicted in Fig. 6a. The circular shape of the SE leads in some way to the evaluation of the curvature of strokes which activate the retina. The set $X^c$ shown in Fig. 8a corresponds to the complement of signal $X$ in the circular domain $E$ defined by the circumscribing circle to the border of retina $W$ (Fig. 5). The first components $p(n)$ of the pseudopecstrum $\Psi p_s(X^c)$ (Fig. 8b) reflect both the curvature of the writing trace of the signature and the manner in which the signal $X$ covered the area of the retina. The impulses located at the end of the scale of the

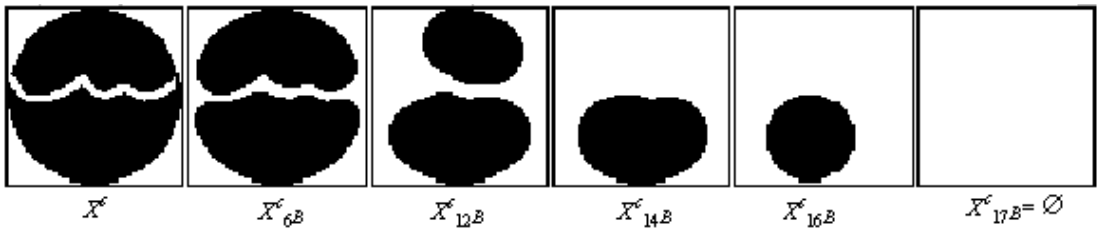


(a)

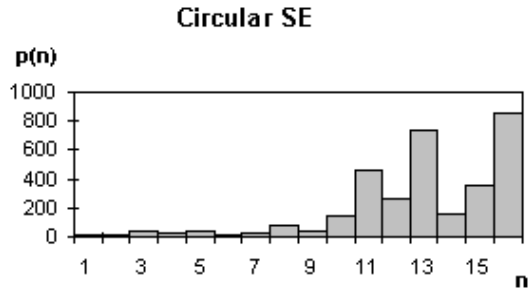


(b)

Fig. 8. Pseudopecstrum $\Psi p_S(X^C)$ based on a circular SE {•} (b) has been applied to the same retina *W* shown in Fig. 6a. Several openings of set $X^C$ are also depicted in (a).

pseudopecstrum are related to the measurement of parts of set $X^c$ located in $(E \cap W)^c$. For example, see the sets $X^c_{12B}$, $X^c_{14B}$, and $X^c_{16B}$ shown in Fig. 8a. Each type of transformation $\Psi(\cdot)$ and the definition of the field of retinas (e.g., the number of foci of attention on the image and the dimension $h \times v$ of each retina) will have a great impact on the performance of the resulting shape descriptor. These parameters will be analyzed in depth in Section 5.1.

## 4 Experimental Protocol and Signature Database Description

### 4.1 Description of the Signature Database

In the field of signature verification, no international database is available due to the confidentiality of this type of data. The proposed signature verification system was tested using a signature database of 800 images consisting of 40 signatures written by 20 individuals. This signature database was built at our laboratory and is used for the evaluation of several signature representation and verification schemes [11], [12], [20], [27], [28], [29], [30], [31], [32], [33]. The signatures were handwritten in a 3 × 12 cm rectangle, using the same type of writing tool (a Pilot Fineliner with flexible felt tip and black ink) and sheets of white paper. Each writer had instructions to write three to four signatures each day during a time frame of two weeks. All images were digitized with a vidicon camera and a frame grabber set to a resolution of 200 dpi. Let $\boldsymbol{R}$ be the reference database related to the first 20 signatures of each writer ($|\boldsymbol{R}| = 400$) and $\boldsymbol{T}$ be the test database which is related to the last 20 signatures of each writer with $|\boldsymbol{T}| = 400$.

### 4.2 Definition of Individual Classifiers and Related Datasets

Two types of classifier were used in this study: a *Nearest Neighbor* (*NN*) *classifier with vote* and a *minimum distance classifier*. The former allows the evaluation of the discriminant power of a shape factor (signature representation R(γ)): This can be related to a lower limit of the total error rate when all the available information is stored in memory. The latter is a more realistic solution to the verification problem, but requires the evaluation of a comparison threshold $\tau^{(i)}$ for each writer enrolled in the verification system. Both classifiers and training procedures are fully described in [30] and [31]. Let $\chi$ be the set of all feature vectors related to a specific representation R(γ), with $|\chi| = 800$. The size of each feature vector $\mathcal{X}_i \in \mathcal{X}$ varies from N = 96 to N = 768 (Table 1), following the definition of the shape factor used for the implementation of each individual classifier (Section 3).

We now define the sets required for evaluating the performance of the classifiers assigned to each writer (*i*), $i = 1, ..., 20$. Let the set of genuine signatures $S^{(i)}_{ref} \subset R^{(i)}$ required as reference signatures be retained for the minimum-distance classifier with threshold $\tau^{(i)}$. The cardinality of this comparison set will be $\left|S^{(i)}_{ref}\right| = N_{ref}$. The comparison signatures are chosen randomly in the reference set $R^{(i)}$ with $\left|R^{(i)}\right| = 20$, and their number is varied within the $1 \le N_{ref} \le 10$ range. Let the learning set $S^{(i)}_{learn} \subset R$ of cardinality $\left|S^{(i)}_{learn}\right| = N_{learn}$ be used for evaluating the threshold $\tau^{(i)}$ for writer (*i*). The learning set $S^{(i)}_{learn}$ is defined by the

TABLE 2
EXPERIMENTAL RESULTS USING THE POSITIVE PECSTRUM $\Psi P(X)$ (ONE ITERATION)

| $h \times v$ $O_h$ $O_v$ | {—} $\varepsilon_t(\%)$ | {\|} $\varepsilon_t(\%)$ | {/} $\varepsilon_t(\%)$ | {\} $\varepsilon_t(\%)$ |
|---|---|---|---|---|
| 16 × 16 0% 0% | 1.19 | 1.04 | 1.68 | 2.64 |
| 0% 50% | 1.30 | 3.32 | 0.94 | 2.47 |
| 50% 0% | 3.33 | **0.59** | **0.48** | 1.37 |
| 50% 50% | 3.32 | 2.77 | 1.19 | 1.46 |
| 16 × 32 0% 0% | 1.66 | 4.17 | 1.66 | 3.30 |
| 0% 50% | 2.18 | 6.01 | 1.49 | 4.09 |
| 50% 0% | 3.06 | 2.04 | 1.62 | 1.96 |
| 50% 50% | 3.45 | 4.56 | 1.48 | 1.69 |
| 32 × 16 0% 0% | 3.66 | 0.72 | 1.02 | 1.50 |
| 0% 50% | 3.32 | 2.18 | 1.79 | 1.90 |
| 50% 0% | 5.47 | **0.39** | **0.49** | 1.34 |
| 50% 50% | 4.63 | 2.51 | 1.52 | 1.74 |
| 32 × 32 0% 0% | 4.86 | 3.67 | 1.99 | 2.53 |
| 0% 50% | 4.65 | 3.95 | 3.20 | 2.97 |
| 50% 0% | 6.46 | 3.52 | 1.32 | 1.61 |
| 50% 50% | 6.45 | 4.20 | 1.88 | 1.61 |
| 64 × 32 0% 0% | 9.96 | 4.45 | 3.63 | 3.34 |
| 0% 50% | 8.81 | 4.32 | 3.19 | 2.91 |
| 50% 0% | 7.73 | 5.14 | 2.08 | 2.43 |
| 50% 50% | 7.67 | 4.53 | 3.13 | 2.51 |

genuine signatures of writer ($i$) that were not chosen in $S_{ref}^{(i)}$ (class $\omega_1$), and by five signatures chosen randomly from all sets $R^{(j)}$ for other writers ($j$) with $1 \le j \le 20, i \ne j$; that is, $5 \times 19$ random forgeries related to class $\omega_2$. In the case of the $NN$ classifier, only the learning set $S_{learn}^{(i)}$ is required, with $N_{learn} = 115$, that is, all 20 observations from class $\omega_1$, and the 95 observations from class $\omega_2$, have been taken into account. The set $S_{gen}^{(i)} \subset T$ is used for the evaluation of the performance in generalization of each classifier, with $\left|S_{gen}^{(i)}\right| = N_{gen}$. Set $S_{gen}^{(i)}$ is made up of 20 genuine signatures from the test set $T^{(i)}$ of writer ($i$) (class $\omega_1$), and by five signatures chosen randomly from all sets $T^{(j)}$ of other writers (j) with $1 \le j \le 20, i \ne j$; that is to say, 5 × 19 random forgeries related to class $\omega_2$; consequently, $\left|S_{gen}^{(i)}\right| = N_{gen} = 115$. Thus, a statistical independence of sets $S_{gen}^{(i)}$, $S_{ref}^{(i)}$, and $S_{learn}^{(i)}$ is always guaranteed because the initial sets $R$ and $T$ satisfy this property.

### 4.3 Definition of Integrated Classifier $E(x)$

Recall from Section 1, that the feature vectors have a high dimension; the number of reference signatures already available for training is normally very low (three to six in practice); and the genuine signature shape is characterized by high intra-class variability over time. As we know, the design of a signature verification system based on a single shape factor or a single shape representation is not a trivial task [33]. One solution is to design a class of shape factor and to build an integrated classifier permitting the cooperation of several classifiers. Combining classifiers is not new in the field of pattern recognition and has been investigated by several authors working in the field of character recognition [14], [37]. Several methods have been proposed and evaluated, but the *voting principle* seems more appropriate for the signature verification problem because one integrated classifier has to be designed for each writer [33]. In character recognition, the design of complex methods for classifier cooperation is justified because only one integrated classifier is required for the implementation of recognition systems. As an example, the implementation of integrated classifiers based on the Bayesian or on Dempster-Shafer theory leads to the proper weighting of individual classifiers and enhances the global reliability of the recognition system [37]. These approaches require a learning procedure for each individual classifier, and a second learning phase for implementing the combining stage of the integrated classifier or for evaluating the performance in generalization of individual classifiers. So, these approaches are intractable in the case of the signature verification problem because the cardinality of the datasets available for training is always small. Here, the $K$ individual classifiers are all of the same type: *NN* or *minimum distance* classifiers based on a transformation $\Psi(\cdot)$ related to the positive pecstrum, the pseudopecstrum or the augmented pseudopecstrum using SE in the set {|, —, /, \}. In the case of integrated classifiers $E(x)$ based on $K = 4$ individual classifiers [33], a value of $\alpha = 0.75$ corresponds to the simple majority rule and a value of $\alpha = 1.0$ states that a decision made by an integrated classifier $E(x)$ requires the unanimity of all individual classifiers.

TABLE 3
EXPERIMENTAL RESULTS USING THE PSEUDOPECSTRUM $\Psi p_s(X^c)$ (ONE ITERATION)

| $h \times v$ $O_h$ $O_v$ | {—} $\varepsilon_t(\%)$ | {\|} $\varepsilon_t(\%)$ | {/} $\varepsilon_t(\%)$ | {\} $\varepsilon_t(\%)$ | {•} $\varepsilon_t(\%)$ |
|---|---|---|---|---|---|
| $16 \times 16$ 0% 0% | 0.36 | 0.45 | 4.16 | 0.71 | 0.00 |
| 0% 50% | 0.03 | 0.36 | 6.46 | 1.48 | 0.15 |
| 50% 0% | 0.30 | 0.15 | 1.82 | 1.11 | 0.03 |
| 50% 50% | 0.00 | 0.00 | 0.99 | 0.08 | 0.15 |
| $16 \times 32$ 0% 0% | 0.48 | 0.68 | 4.25 | 1.71 | 0.00 |
| 0% 50% | 0.18 | 0.76 | 1.07 | 0.63 | 0.00 |
| 50% 0% | 0.15 | 0.08 | 2.91 | 0.34 | 0.18 |
| 50% 50% | 0.18 | 0.13 | 0.23 | 0.15 | 0.00 |
| $32 \times 16$ 0% 0% | 0.71 | 0.30 | 2.72 | 2.48 | 0.03 |
| 0% 50% | 0.03 | 0.28 | 1.35 | 0.45 | 0.15 |
| 50% 0% | 0.20 | 0.03 | 0.30 | 0.15 | 0.13 |
| 50% 50% | 0.00 | 0.00 | 0.36 | 0.96 | 0.40 |
| $32 \times 32$ 0% 0% | 0.30 | 0.46 | 4.44 | 1.40 | 0.18 |
| 0% 50% | 0.20 | 0.33 | 1.14 | 0.38 | 0.05 |
| 50% 0% | 0.11 | 0.00 | 0.84 | 1.02 | 0.33 |
| 50% 50% | 0.00 | 0.15 | 0.59 | 0.20 | 0.20 |
| $64 \times 32$ 0% 0% | 0.38 | 0.43 | 2.15 | 2.17 | 0.90 |
| 0% 50% | 0.11 | 0.30 | 2.16 | 0.31 | 0.20 |
| 50% 0% | 0.28 | 0.03 | 0.18 | 0.34 | 1.12 |
| 50% 50% | 0.00 | 0.30 | 0.43 | 0.33 | 0.53 |

TABLE 4
EXPERIMENTAL RESULTS USING THE AUGMENTED PSEUDOPECSTRUM $\Psi ap_s(X^c)$ (ONE ITERATION)

| $h \times v$ $O_h$ $O_v$ | {—} $\varepsilon_t(\%)$ | {\|} $\varepsilon_t(\%)$ | {/} $\varepsilon_t(\%)$ | {\} $\varepsilon_t(\%)$ |
|---|---|---|---|---|
| $16 \times 16$ 0% 0% | 0.13 | 0.03 | 2.31 | 0.33 |
| 0% 50% | 0.15 | 0.13 | 0.68 | 1.07 |
| 50% 0% | 0.00 | 0.00 | 0.81 | 1.47 |
| 50% 50% | 0.00 | 0.13 | 0.20 | 0.00 |
| $16 \times 32$ 0% 0% | 0.15 | 0.18 | 0.87 | 2.30 |
| 0% 50% | 0.15 | 0.13 | 0.18 | 0.13 |
| 50% 0% | 0.00 | 0.00 | 0.45 | 0.00 |
| 50% 50% | 0.03 | 0.03 | 0.00 | 0.15 |
| **$32 \times 16$** 0% 0% | 0.13 | 0.03 | 1.16 | 1.80 |
| 0% 50% | 0.15 | 0.25 | 0.63 | 0.13 |
| **50% 0%** | **0.00** | **0.00** | **0.00** | **0.00** |
| 50% 50% | 0.03 | 0.00 | 0.13 | 0.13 |
| $32 \times 32$ 0% 0% | 0.13 | 0.13 | 1.17 | 0.48 |
| 0% 50% | 0.13 | 0.00 | 0.03 | 0.41 |
| 50% 0% | 0.00 | 0.00 | 0.23 | 0.66 |
| 50% 50% | 0.05 | 0.13 | 0.20 | 0.13 |
| $64 \times 32$ 0% 0% | 0.15 | 0.13 | 1.70 | 1.49 |
| 0% 50% | 0.15 | 0.51 | 0.91 | 0.36 |
| 50% 0% | 1.45 | 0.08 | 0.33 | 0.41 |
| 50% 50% | 0.30 | 0.33 | 0.51 | 0.56 |

TABLE 5
EXPERIMENTAL RESULTS USING THE AUGMENTED PSEUDOPECSTRUM $\Psi ap_s(X^c)$ AND THE NN CLASSIFIER (25 ITERATIONS)

| SE | $\bar{\varepsilon}_1(\%)$ $(\pm\sigma)(\%)$ | $\bar{\varepsilon}_2(\%)$ $(\pm\sigma)(\%)$ | $\bar{\varepsilon}_t(\%)$ $(\pm\sigma)(\%)$ |
|---|---|---|---|
| {—} | 0.00 (0.00) | 0.04 (0.04) | 0.02 (0.02) |
| {\|} | 0.00 (0.00) | 0.04 (0.05) | 0.02 (0.02) |
| {/} | 0.00 (0.00) | 0.04 (0.04) | 0.02 (0.02) |
| {\} | 0.00 (0.00) | 0.03 (0.04) | 0.02 (0.02) |
| {•} | 0.20 (0.14) | 0.15 (0.09) | 0.18 (0.08) |

TABLE 6
EXPERIMENTAL RESULTS USING THE AUGMENTED PSEUDOPECSTRUM $\Psi ap_s(X^c)$ AND THE MINIMUM DISTANCE CLASSIFIER (25 ITERATIONS) WITH $N_{ref} = 6$

| SE | $\bar{\varepsilon}_1(\%)$ $(\pm\sigma)(\%)$ | $\bar{\varepsilon}_2(\%)$ $(\pm\sigma)(\%)$ | $\bar{\varepsilon}_t(\%)$ $(\pm\sigma)(\%)$ |
|---|---|---|---|
| {—} | 1.55 (0.55) | 0.15 (0.15) | 0.85 (0.26) |
| {\|} | 2.67 (0.75) | 0.48 (0.19) | 1.58 (0.37) |
| {/} | 3.01 (0.68) | 0.32 (0.20) | 1.66 (0.35) |
| {\} | 2.07 (0.83) | 0.31 (0.19) | 1.19 (0.42) |

TABLE 7
EXPERIMENTAL RESULTS USING THE AUGMENTED PSEUDOPECSTRUM $\Psi ap_s(X^c)$ WITH STRUCTURING ELEMENTS {—, |, /, \} (25 ITERATIONS) AND THE NN-BASED INTEGRATED CLASSIFIER

| decision threshold | $\bar{\varepsilon}_1(\%)$ $(\pm\sigma)(\%)$ | $\bar{\varepsilon}_2(\%)$ $(\pm\sigma)(\%)$ | $\bar{\varepsilon}_t(\%)$ $(\pm\sigma)(\%)$ | $\bar{R}_1(\%)$ $(\pm\sigma)(\%)$ | $\bar{R}_2(\%)$ $(\pm\sigma)(\%)$ | $\bar{R}_t(\%)$ $(\pm\sigma)(\%)$ |
|---|---|---|---|---|---|---|
| $\alpha = 0.75$ | 0.00 (0.00) | 0.02 (0.03) | **0.01** (0.01) | 0.00 (0.00) | 0.02 (0.03) | **0.01** (0.01) |
| $\alpha = 1.0$ | 0.00 (0.00) | 0.00 (0.01) | **0.00** (0.01) | 0.00 (0.00) | 0.09 (0.08) | **0.05** (0.04) |

TABLE 8
EXPERIMENTAL RESULTS USING THE AUGMENTED PSEUDOPECSTRUM $\Psi ap_s(X^c)$ WITH STRUCTURING ELEMENTS {—, |, /, \} (25 ITERATIONS) AND THE MINIMUM-DISTANCE-BASED INTEGRETED CLASSIFIER WITH $N_{ref} = 6$

| decision threshold | $\bar{\varepsilon}_1(\%)$ $(\pm\sigma)(\%)$ | $\bar{\varepsilon}_2(\%)$ $(\pm\sigma)(\%)$ | $\bar{\varepsilon}_t(\%)$ $(\pm\sigma)(\%)$ | $\bar{R}_1(\%)$ $(\pm\sigma)(\%)$ | $\bar{R}_2(\%)$ $(\pm\sigma)(\%)$ | $\bar{R}_t(\%)$ $(\pm\sigma)(\%)$ |
|---|---|---|---|---|---|---|
| $\alpha = 0.75$ | 1.64 (0.70) | 0.1 (0.11) | **0.87** (0.33) | 1.01 (0.47) | 0.22 (0.13) | **0.62** (0.25) |
| $\alpha = 1.0$ | 0.52 (0.44) | 0.02 (0.06) | **0.27** (0.22) | 3.97 (0.95) | 0.79 (0.26) | **2.38** (0.49) |

## 5 EXPERIMENTATION

### 5.1 Prototyping Phase

All representations R(γ) that were defined in Section 3 were evaluated using an *NN classifier with vote*. For each classifier tailored for a representation R(γ), the performance of the verification system is reported in terms of Type I ($\varepsilon_1$, false rejection of genuine signatures) and Type II ($\varepsilon_2$, false acceptance of random forgeries) error rates evaluated for the 20 writers. The average total error rate $\varepsilon_t$ of a verification system is expressed in terms of Type I and Type II error rates, as $\varepsilon_t = (\varepsilon_1 + \varepsilon_2) / 2$. In this experiment, the comparison of several strategies was made on the basis of $\varepsilon_t$ values.

The positive pattern spectrums $\Psi p(X)$ based on an SE in {|, —, /, \} was evaluated first using several definitions of retinas $W$ (Table 1) and of percentages of overlap $O_h$ and $O_v$ between retinas. Table 2 shows that better results were obtained with rectangular windows whose longest side is the horizontal one; as an example, see the results obtained with $|W| = 32 \times 16$ and 50 percent of overlap $O_h$. In the second set of experiments, the pseudopecstrum $\Psi p_s(X^c)$ based on an SE in {|, —, /, \, •} was used with the same set of retinas as above. The general trend in the data shows a substantial decrease in the average error rate for all types of retinas, except for the smaller ones (Table 3). This phenomenon tells us that, for the class of signals $X$ under study, the strokes

can be characterized more efficiently by measurements made on the background in the field of view of the retina $W$. This confirms that only small amounts of information are conveyed by the positive pattern spectrum, because the measurements are made inside the writing trace of the signature. Following these experiments, the augmented pseudopecstrums $\Psi ap_s(X^c)$ based on SE in {|, —, /, \} were used in an attempt to evaluate the influence of border effects produced by pixels in $X$ located in the neighborhood of the external border of $W$. Again, the performance of the majority of schemes is better than the approaches listed in Table 4. Based on these experimental results, a rectangular retina $W$ of 32 × 16 pixels with $O_h$ = 50 percent of overlap was retained for the final implementation of a signature verification system, because a perfect recognition rate has been achieved for each SE.

### 5.2 Evaluation of the Performance of Individual Classifiers

The above experiments using the augmented pseudopecstrums $\Psi ap_s(X^c)$ based on SE in {|, —, /, \} and the one using the pseudopecstrum $\Psi p_s(X^c)$ based on circular SE {•} were repeated 25 times for each signature verification system; the observations of class $\omega_2$, the subsets of $S_{learn}^{(i)}$ and $S_{gen}^{(i)}$, were regenerated randomly each time, following our standard protocol [30], [31], [32], [33]. Randomly redefining the datasets at each iteration in some way permits measurement of the variability of handwriting from one experiment to an other. In the case of the *minimum distance classifier*, the effect on the global performance of the choice and number of reference signatures (class $\omega_1$) (Section 4.2) in the definition of sets $S_{ref}^{(i)}$ was also taken into account. The average performances $\overline{\varepsilon_t}$ of the signature verification systems, resulting from the performances on 25 iterations of representations R(γ), and used for both types of classifiers, are depicted in Tables 5 and 6. At first glance, it is clear that the verification systems built around *NN* classifiers outperform those based on *minimum distance* classifiers for all representations R(γ) under study. As an example, $\overline{\varepsilon_t}$ varies in the range of values (0.02 percent - 0.18 percent) for the *NN* classifier Table 5 and in the range of values (0.85 percent - 1.66 percent) for the *minimum distance* classifier using $N_{ref}$ = 6 reference signatures Table 6. The experimental results shown in Fig. 9 illustrate the effect of the number of reference signatures for each minimum-distance classifier evaluated in this experiment, for $1 \le N_{ref} \le 10$. We see that the performance obtained for each structuring element is almost the same for $N_{ref} \ge 4$ reference signatures. We retain the value of $N_{ref}$ = 6 to be able to compare the performance of the proposed approach with other works, using the same experimental protocol and the same datasets [28], [29], [30], [31], [32], [33].

One last comment about the circular SE {•}: It was decided that transformations $\Psi p_s(X^c)$ based on this SE be discarded because the performance obtained with the NN classifier is not as good than the performance obtained with SE in {|, —, /, \}, and because the evaluation of the pseudopecstrums on big retinas is too time-consuming. A factor of 10 in computer time has be observed on average for the circular SE {•} compared to the worst case related to the horizontal SE {—}.

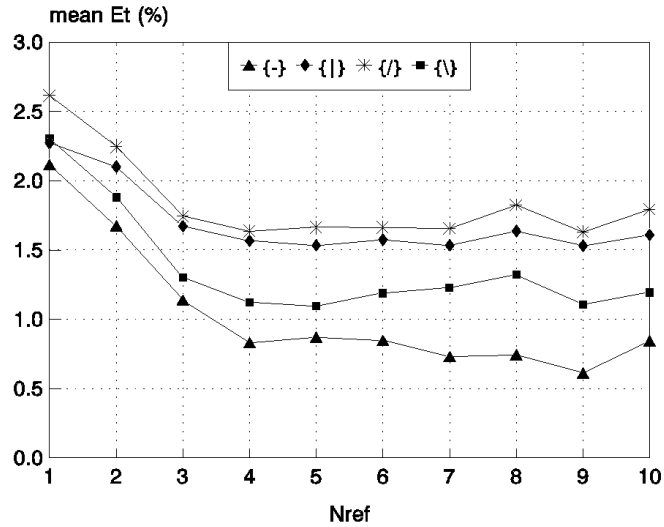


Fig. 9. Evaluation of verification systems based on minimum distance classifiers with $1 \le N_{ref} \le 10$.

### 5.3 Evaluation of Integrated Classifier Performance

In practice, the choice of the best representation R(γ) for the implementation of a signature verification system is a very difficult task because the amount of data available is always very small, especially in the case of reference signatures related to class $\omega_1$. For this reason, the design of integrated classifiers $E(x)$ based on a large number of individual classifiers (or signature representations R(γ)) could be a nice solution to the problem of overcoming the need for feature selection [33].

Experimental results obtained using the simple majority rule ($\alpha$ = 0.75) and the unanimity rule ($\alpha$ = 1.0) were obtained for both types of integrated classifiers $E(x)$ discussed in Section 4.3. In both cases, the integrated classifiers $E(x)$ are based on four individual classifiers of the same type, either the *NN* or the minimum distance classifier. From a practical point of view, this architecture can be implemented easily on a parallel machine, e.g., one processor per classifier. In that case, the total processing time will be reduced to that of the slowest classifier. Moreover, considering that each representation R(γ) used the same retina definition of 32 × 16 pixels with $O_h$ = 50 percent overlap ($|W|$ = 64 × 16 pixels), several retinas could be analyzed simultaneously if a multi-processor machine were available. The results obtained with the *NN*-based integrated classifier are encouraging, considering the very low rejection rate observed when the unanimity rule is used Table 7, which shows an $\overline{\varepsilon_t} \cong 0$ percent for a mean rejection rate of $\overline{R_t}$ = 0.05 percent. The price to pay in this case is the large amount of data

$$\left(\left|S_{learn}^{(i)}\right| = 115 \text{ reference signatures}\right)$$

kept in memory for each writer ($i$). It is normal to observe a worst performance using the minimum-distance-based integrated classifier (Table 8). But the results shown in Table 8 are the best experimental results already published using this experimental protocol and this database with $\overline{\varepsilon_t}$ = 0.87 percent and $\overline{R_t}$ = 0.62 percent using the simple majority rule ($\alpha$ = 0.75). This result is as good as the one obtained with the best individual classifier based on the SE {—} Table 6. In the case of integrated classifiers $E(x)$ using the unanimity rule, the experimental results are quite good considering that the rejection rate is below 5 percent [12], that is, $\overline{\varepsilon_t}$ = 0.27 percent and $\overline{R_t}$ = 2.38 percent.

## 6 Conclusion

A new approach based on visual perception has been proposed in an attempt to define a shape factor tailored for the signature-verification problem in the context of random forgeries. Focusing the attention on fixed regions in the 2D space and restricting the field of view of the retinas leads to a representation of the signature based on a local analysis of the scene without the need to segment the writing trace of the signature into primitives. Moreover, evaluating the amount of signal activity using morphological operators applied to the background area, i.e., to $X^c$, in some way permits measurement of the natural local variations of the writing trace of the signature which is closely related to the identity of the writer. Despite the fact that the approach shown in this paper seems very promising, it should be validated on a large signature database where several types of signatures can be taken into account (North American, European, Arabic, Chinese, etc).

Further work is needed to find a mechanism capable of incorporate other measurements that depend on the complexity of the image under study. A dynamic definition of the position and size of the retinas based on the context of the scene is of interest. The cooperation of several classifiers will be extended towards a local cooperation of morphological operators acting on a retina. This will shift the data fusion from the decision level towards the feature extraction level.

## Acknowledgments

We would like to thank Caroline Baillard and Olivier Coulon who participated in the implementation of the algorithms for the definition and evaluation of a new shape factor based on morphological transformations. Special thanks to the two referees for their constructive comments and suggestions. This work was supported in part by grant OGP0106456 to Robert Sabourin from the NSERC of Canada.

## References

[1] M. Ammar, Y. Yoshida, and T. Fukumura, "Off-Line Preprocessing and Verification of Signatures," *Int'l J. Pattern Recognition and Artificial Intelligence*, vol. 2, no. 4., pp. 589-602, 1988.

[2] V. Anastassopoulos and A.N. Venetsanopoulos, "The Classification Properties of the Pecstrum and Its Use for Pattern Identification," *Circuits Systems Signal Process*, vol. 10, no. 3, pp. 293-326, 1991.

[3] C. Baillard, "Les Techniques de Spectres de Formes et de Moments Granulométriques Appliquées à la Vérification de Signatures Manuscrites - Approche Globale," *Rapport de Stage de 3e année*. Paris: Telecom-Paris, 1994.

[4] S.N. Biswas and B.B.Chaudhuri, "On the Generation of Discrete Circular Objects and Their Properties," *Computer Vision, Graphics, and Image Processing*, no. 32, pp. 158-170, 1985.

[5] E.R. Brocklehurst, "Computer Methods of Signature Verification," *J. Forensic Science Society*, pp. 445-457, 1985.

[6] J.F. Bronskill and A.N. Venetsanopoulos, "Multidimensional Shape Description and Recognition Using Mathematical Morphology," *J. Intelligent and Robotic Systems*, vol. 1, pp. 117-143, 1988.

[7] O. Coulon, "Les Techniques de Spectres de Formes et de Moments Granulométriques Appliquées à la Vérification de Signatures Manuscrites—Approche Locale, "*Rapport de Stage de 3e année*. Paris: Telecom-Paris, 1994.

[8] E. Dougherty, "Pattern Spectrum and Granulometric Moments," *Morphological Image Processing*, E. Dougherty ed. New York: Marcel Dekker Inc., 1992.

[9] E. Dougherty, J. Pelz, F. Sand, and A. Lent, "Morphological Image Segmentation by Local Granulometric Size Distributions," *J. Electronic Imaging*, vol. 1, no. 1, pp. 46-60, Jan. 1992.

[10] E. Dougherty, Y. Chen, J. Hornak, and S. Totterman, "Detection of Osteoporosis by Morphological Granulometries," *Proc. SPIE*, vol. 1,660, Feb. 1992.

[11] J.P. Drouhard, R. Sabourin, and M. Godbout, "Evaluation of a Training Method and of Various Rejection Criteria for a Neural Network Classifier Used for Off-Line Signature Verification," *IEEE Int'l Conf. Neural Networks*, Orlando, Fla., June 26-July 2, pp. 4,294-4,299, 1994.

[12] J.P. Drouhard, R. Sabourin, and M. Godbout, "A Neural Approach to Off-Line Signature Verification Using Directional PDF," *Pattern Recognition*, vol. 29, no. 3, pp 415-424, Mar. 1996.

[13] W.R. Harrison, *Suspect Documents, Their Scientific Examination*. Chicago: Nelson-Hall Publishers, 1981.

[14] Y.S. Huang and C.Y. Suen, "Combination of Multiple Classifiers with Measurement Values," *Proc. Second IAPR Conf. Document Analysis and Recognition*, Tsukuba, Japan, pp. 598-601, Oct. 1993.

[15] F. Leclerc and R. Plamondon, "Automatic Signature Verification: The State of the Art—1989-1993," *Int'l J. Pattern Recognition and Artificial Intelligence*, Special Issue on Automatic Signature Verification, pp. 3-20, 1994.

[16] M.D. Levine, *Vision in Man and Machine*. New York: McGraw-Hill, 1985.

[17] E. Locard, "Les Faux en Écriture et leur Expertise," *Payot*, Paris, 1959.

[18] P. Maragos, "Pattern Spectrum and Multiscale Shape Representation," *IEEE Trans. Pattern Analysis and Machine Intelligence*, vol. 11, no. 7, pp. 701-716, July 1989.

[19] G. Matheron, *Random Sets and Integral Geometry*. New York: Wiley and Sons, 1975.

[20] N.A. Murshed, F. Bortolozzi, and R. Sabourin, "Off-Line Signature Verification, Without a Priori Knowledge of Class $\omega_2$. A New Approach, "*Proc. Third IAPR Conf. Document Analysis and Recognition*, pp. 191-196, Aug. 14-16, Montréal, Canada, pp. 191-196, 1995.

[21] R.N. Nagel and A. Rosenfeld, "Computer Detection of Freehand Forgeries," *IEEE Trans. Computers*, vol. 26, no. 9, pp. 895-905, 1977.

[22] W.F. Nemcek and W.C. Lin, "Experimental Investigation of Automatic Signature Verification," *IEEE Trans. Systems, Man and Cybernetics*, pp. 121-126, 1974.

[23] F. Nouboud and R. Plamondon, "Global Parameters and Curves for Off-Line Signature Verification," *Proc. Int'l Workshop on Frontiers in Handwriting Recognition*, Taiwan, pp. 145-155, 1994.

[24] R. Plamondon and G. Lorette, "Automatic Signature Verification and Writer Identification—The State of the Art," *Pattern Recognition*, vol. 22, no. 2, pp. 119-128, 1989.

[25] J. Mathyer, "The Expert Examination of Signatures," *J. Criminal Law, Criminology, and Police Science*, vol. 5, no. 3, May-June, pp. 122-133, 1961.

[26] Y. Qi and B.R. Hunt, "Signature Verification Using Global and Grid Features," *Pattern Recognition*, vol. 27, no. 12, pp. 1,621-1,629, 1994.

[27] R. Sabourin, "Une Approche de Type Compréhension de Scène Appliquée au Problème de la Vérification Automatique de L'Identité par L'Image de la Signature Manuscrite," Thèse de PhD, École Polytechnique de Montréal, Dec. 1990.

[28] R. Sabourin, R. Plamondon, and G. Lorette, "Off-Line Identification with Handwritten Signature Images: Survey and Perspectives," *Structured Document Image Analysis*. New York: Springer-Verlag, pp. 219-234, 1992.
[29] R. Sabourin and J.P. Drouhard, "Off-Line Signature Verification Using Directional PDF and Neural Networks," *Proc. of the 11th ICPR*, pp. 321-325, The Hague, The Netherlands, 1992.
[30] R. Sabourin, M. Cheriet and G. Genest, "An Extended-Shadow-Code Based Approach for Off-Line Signature Verification," *Second IAPR Conf. Document Analysis and Recognition*, pp. 1-5,Tsukuba, Japan, Oct. 1993.
[31] R. Sabourin, R. Plamondon, and L. Beaumier, "Structural Interpretation of Handwritten Signature Images," *Int'l J. Pattern Recognition and Artificial Intelligence*, Special Issue on Automatic Signature Verification, pp. 709-748, 1994.
[32] R. Sabourin and G. Genest, "An Extended-Shadow-Code Based Approach for Off-Line Signature Verification: Part 1—Evaluation of The Bar Mask Definition, "*12th ICPR*, Jerusalem, Israel, Oct. 9-13, vol. 2, pp. 450-453, 1994.
[33] R. Sabourin and G. Genest, "An Extended-Shadow-Code Based Approach for Off-Line Signature Verification: Part 2—Evaluation of Several Multi-Classifier Combination Strategies, "*Third IAPR Conf. Document Analysis and Recognition*, pp. 197-201, Montréal, Canada, Aug. 14-16, 1995.
[34] M. Schmitt and J. Mattioli, "Reconnaissance de Formes Planaires par Morphologie Mathématique et Réseaux de Neurones," *Revue Technique Thomson-CSF*, vol. 22, no. 4, pp. 573-609, Dec. 1990.
[35] J. Serra, *Image Analysis and Mathematical Morphology*. New York: Academic Press, 1982.
[36] T.S. Wilkinson and J.W. Goodman, "Slope Histogram Detection of Forged Handwritten Signatures," *Proc. SPIE*, pp. 293-304, Boston, 1990.
[37] L. Xu, A. Krzyzak, and C.Y. Suen, "Methods of Combining Multiple Classifiers and Their Applications to Handwriting Recognition," *IEEE Trans. SMC*, vol. 22, no. 3, pp. 418-435, 1992.

**Robert Sabourin** received BIng, MScA, and PhD degrees in electrical engineering from the École Polytechnique de Montréal in 1977, 1980, and 1991, respectively. In 1977, he joined the Physics Department of the Université de Montréal where he was responsible for the design and development of scientific instrumentation for the Observatoire du Mont Mégantic. In 1983, he joined the staff of the École de Technologie Supérieure, Université du Québec, Montréal, P.Q., Canada, where he is currently a professeur titulaire in the Département de Génie de la Production Automatisée. Since 1996, he has been a member of the Centre for Pattern Recognition and Machine Intelligence (CENPARMI, Concordia University). His research interests are in the areas of handwriting recognition and signature verification for banking and postal applications.

**Ginette Genest** received a BSc in biology, and a BScA in electrical engineering from Laval University in 1977 and 1980, respectively. For the last five years, she has been a research assistant in the Département de Génie de la Production Automatisée of the École de Technologie Supérieure. Her research interests are in the areas of pattern recognition and computer vision.

**Françoise J. Prêteux** is currently a professor, and head of the Department of Signal and Image Processing at the Institut National des Télécommunications, Evry, France, which she created in 1994. Her research activities lie in the fields of pattern recognition, image analysis and, more specifically, stochastic modeling, mathematical morphology, and scene deformation analysis.

She is a member of the editorial board of the *Journal of Electronic Imaging*, and is cochair of the Statistical and Stochastic Methods for Image Processing Conference (SPIE). She also serves on numerous conference committees associated with the professional organizations in this field.

Dr. Prêteux graduated from the Ecole des Mines de Paris (1982) and received her thèse d'état in mathematics from the Université de Paris VI (1987). Before joining INT, she worked as a research engineer at the Mathematical Morphology Center of Fontainebleau and was a consultant for several industrial companies (1982-1989). She then held a position as professor in the Image Processing Department at the Ecole Nationale Supérieure des Télécommunications (1989-1993).